Optical Fréedericksz transition in liquid crystals and transfer of the orbital angular momentum of light

Bruno Piccirillo,* Angela Vella,† and Enrico Santamato‡
Istituto Nazionale di Fisica della Materia, Dipartimento di Scienze Fisiche, via Cintia, 80126 Napoli, Italy
(Received 23 July 2003; published 17 February 2004)

Multistability, out-of-polarization-plane reorientation, and persistent oscillations have been observed in the optical Fréedericks transition in a homeotropically aligned nematic film using a normally incident linearly polarized laser beam with elliptical rather than circular cross section. These features could be ascribed to the presence of an additional optical torque connected with a transfer of the orbital angular momentum of light to the liquid crystal film. A model based on Ritz's variational method confirms this picture.

DOI: 10.1103/PhysRevE.69.021702 PACS number(s): 42.70.Df, 42.65.−k, 61.30.Gd

I. INTRODUCTION

When a linearly polarized laser beam is focused at normal incidence onto a homeotropically aligned nematic film, the reorientation of the molecular director $\boldsymbol{n}$ is induced only when the laser intensity exceeds a characteristic threshold value I_{th}. The transition to the distorted state is usually second order and it is known as the optical Fréedericksz transition (OFT) [1,2]. The OFT is one of the most known and most studied nonlinear optical effects in liquid crystals (LC) (for a review on the subject see, for example, Refs. [3–5]). Above the threshold I_{th}, the distorted state is stable and the distortion increases with the incident laser power P until saturation is reached. The phenomenon is quite similar to the well known Fréedericksz effect observed in nematics in the presence of static electric fields [6]. Bistability and director oscillations were neither reported nor theoretically predicted in the OFT. The possibility of changing the OFT so to obtain two or more steady states at the same incident light power P has attracted much attention in view of potential applications, and several experiments have been considered during the last two decades. Bistability in the OFT was obtained, for example, by applying a second field, either magnetic [7] or optical [8], by adding small amount of cholesteric liquid crystal to the nematic material [9], or by introducing strong external feedback by a Fabry Perot cavity [10] or an optical fiber [11,12]. In the present work, we will prove, among other things, that multiple stable steady states can be obtained by using a laser beam having an elliptical intensity profile. Recent experiments proved, in fact, that the optical reorientation in nematics is dramatically affected by the shape of the incident laser beam [13,14]. In particular, it was observed that when the laser beam had an elliptical rather than circular profile, the LC molecules tend to rotate along the beam z axis until they end up aligned along the major axis of the beam cross section. This aligning effect was found still present when the light beam was completely unpolarized and the z component of the optical torque $\boldsymbol{\tau}^o$ acting on the unit volume $\tau_z^o = (1/8\pi)\mathrm{Re}(\boldsymbol{D}^* \times \boldsymbol{E})_z$ ($\boldsymbol{D}$ and $\boldsymbol{E}$ denote the electric induction and field in Gaussian units, respectively) averages to zero. This proves the existence of a novel, yet unexplored, source of optical torque [13,14]. Soon after, it was suggested that the new source of optical torque could be the transfer to the LC of the z component of the orbital, rather than the spin, angular momentum of light [15].

The aim of the present paper is to investigate in some detail the changes induced in the OFT by the elliptical shape of the laser beam and by the extra torque connected with the orbital angular momentum of light. All measurements were made in the standard configuration for the OFT: normal incidence, linear light polarization, and homeotropic initial alignment of the nematic film. The only difference was that the beam cross section at the film position was set elliptical rather than circular. All observations reported in this work refer to an elliptically shaped laser beam having waists $w_x = 178\ \mu$m and $w_y = 12\ \mu$m at the sample position. In our experiments, the optical reorientation was studied as a function of the laser beam power P and of the angle β between the major axis of the beam intensity profile and the polarization direction. Some observations, as the increase of the OFT threshold with β, were expected, but others were surprising. For example, just above the threshold for the OFT, multiple steady states were observed for $\beta > 10°$, and for $\beta \geqslant 60°$ persistent oscillations of the molecular director arose spontaneously. These phenomena were never reported in the standard OFT with circularly shaped laser beams. The paper is sectioned as follows: in Sec. II, we present a model accounting for the main features of the observed phenomena and stressing the role played by the angular momentum of light in the reorientation process. It is worth noting that usual approximations made in the optics of liquid crystals, namely, the plane-wave and the one-elastic-constant approximations are inadequate in the present case: the transverse coordinates and the elastic anisotropy play here an essential role. This renders the modeling problem very difficult. In Sec. III, our experimental results are presented and compared with the theory. Finally, in Sec. IV, our conclusions are drawn.

II. THE MODEL

Liquid crystals are birefringent materials very sensitive to the polarization of light. The polarization of light is related to the photon spin angular momentum, which therefore can be transferred from the light beam to the LC material. The pos-

*Electronic address: bruno.piccirillo@na.infn.it
†Electronic address: angela.vella@na.infn.it
‡Electronic address: enrico.santamato@na.infn.it

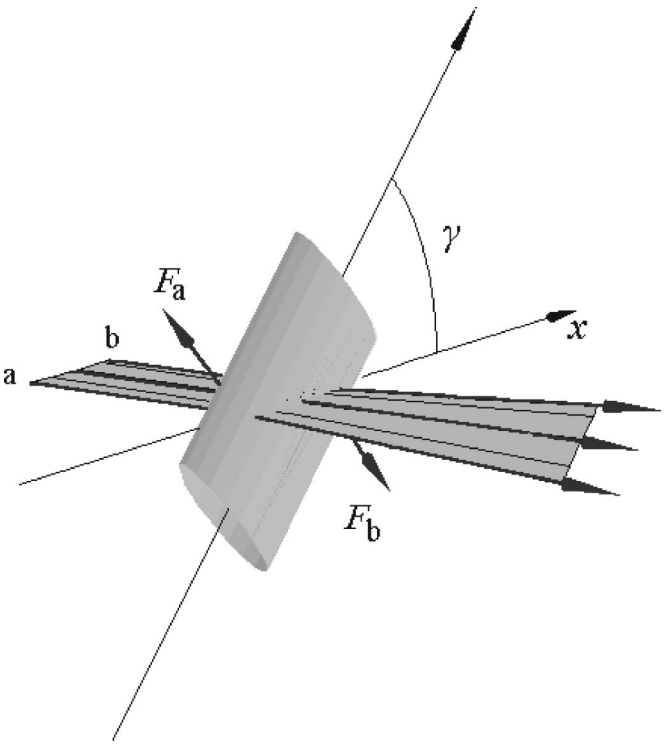

FIG. 1. The reoriented liquid crystal can be considered as a cylindrical microlens. Refraction of the incident beam by this lens results in a couple of forces $\boldsymbol{F}_a$ and $\boldsymbol{F}_b$ acting on the lens itself.

sibility of transferring the spin angular momentum of light to LC was demonstrated in several experiments [16–18] and used, in more recent times, to obtain accurate angular control of the molecular orientation [19]. The possibility of transferring the orbital angular momentum of light was explored only recently [15], although very general variational three-dimensional approaches to the optical distortion in liquid crystals lead to conservation laws including the orbital part of the optical angular momentum [20]. In typical experiments on laser-induced reorientation, the laser beam is focused into the LC sample to a spot of a few hundred microns or less. Above the threshold for the OFT, the optical reorientation is thus confined to a very small region in the focal zone, producing a spatially inhomogeneous distribution of the refractive index. The reoriented LC sample can be assimilated, therefore, to a thin microlens whose index profile may eventually change in time. If the intensity profile of the incident laser beam is elongated, the refractive index profile will be elongated as well, leading to an effective cylindrical-like laser-induced microlens. In general, the axis of the cylindrical microlens may be not aligned with the axis of the beam profile. In these conditions, the refraction of the elliptically shaped laser beam through the microlens may produce a torque on it, as shown in Fig. 1. It is clear from the figure that the couple of forces acting on the lens is due to photon recoil during refraction and, hence, this couple originates from the orbital angular momentum of the light beam. We may expect, therefore, that the LC could be also sensitive to the orbital part of the light angular momentum. The possibility of extracting the orbital angular momentum from the light beam depends crucially on the presence of transverse gradients in the refractive index of the medium. This renders the plane-wave approximation, which works so well to describe the transfer of the optical spin to LC [18], completely inadequate from the very first beginning. Transverse coordinates must be retained in any model aiming at describing the effects due to the orbital angular momentum of light. In this respect, the transfer of the orbital angular momentum from a light beam to a LC film can be regarded as a sort of ''transverse effect.'' Transverse effects in the optical reorientation of LC have been rarely considered in the literature and mainly concerning the increase of the OFT threshold due to the finite cross section of the incident beam [21–23]. In this section, we present a more general approach to transverse effects in the OFT, which allows us to include more delicate phenomena related to the shape of the beam profile, including the transfer of the orbital angular momentum of light.

Let us consider the typical geometry of the OFT: a linearly polarized laser beam is focused at normal incidence onto a homeotropically aligned nematic LC film having thickness L. The only difference with the usual OFT experimental configuration is that we allow for an arbitrary beam intensity profile $I(x,y)$ at the film location. We assume the LC sample so thin that self-focusing as well as deflection of light can be neglected [24]. Hence, the profile $I(x,y)$ is independent of the z coordinate. In our experiments a TEM_{00} laser beam was focused into the sample by two cylindrical lenses having their cylindrical axes aligned along the x and y directions, respectively. We may assume therefore the intensity profile to be Gaussian at the sample position with different waists w_x and w_y:

$$I(x,y)=I_0\, e^{-2(x^2/w_x^2+y^2/w_y^2)}, \tag{1}$$

where $I_0=2P/(\pi w_x w_y)$ and P is the total power carried by the beam. The phase profile of the incident beam is assumed to be uniform over the transverse cross section and its polarization is assumed linear at angle β with respect to the x axis. Without loss of generality we may take $w_x>w_y$. In the case of a linearly polarized beam with circular cross section ($w_x=w_y$) the experimental geometry reduces to that of the standard OFT [2]. We expect, therefore, that also when the beam profile is elliptical no reorientation occurs until the intensity I_0 at the center of the beam reaches a critical threshold value. Very close to the threshold, the laser-induced reorientation is small, and we may assume $n_z\simeq 1$ and consider n_x and n_y as small quantities. Moreover, in view of the homeotropic boundary conditions at $z=0$ and $z=L$, we may take

$$n_x\simeq\theta(x,y,t)\cos\phi(z,t)\sin\left(\frac{\pi z}{L}\right),$$

$$n_y\simeq\theta(x,y,t)\sin\phi(z,t)\sin\left(\frac{\pi z}{L}\right),$$

$$n_z\simeq 1, \tag{2}$$

where $\theta(x,y,t)$ is the small zenithal angle between $\boldsymbol{n}$ and the z axis. Because no transverse boundary conditions are im-

posed on the azimuthal angle ϕ, we may assume it to be uniform in the x,y plane. The homeotropic alignment implies $\partial_z\phi(0,t)=\partial_z\phi(L,t)=0$. The function $\phi(z,t)$ may be expanded in a series of Chebychev polynomials [25] and only the lowest mode retained, yielding

$$\phi(z,t)=\phi_0(t)-2\phi_1(t)\cos\left(\frac{\pi z}{L}\right). \tag{3}$$

The angle $\phi_0(t)$ is the director azimuthal angle averaged over the sample length and the angle $\phi_1(t)$ is proportional to the director torsion $\Delta\phi(t)=\phi(L,t)-\phi(0,t)=4\phi_1(t)$ along the z axis. Because of the homeotropic alignment imposed by the walls, n_x and n_y vanish outside the illuminated region, so we may assume $\theta(x,y,t)$ having a Gaussian elliptical profile too:

$$\theta(x,y,t)=\theta_0(t)e^{-[\boldsymbol{r}\cdot Q(t)\boldsymbol{r}]}, \tag{4}$$

where $Q(t)$ is a 2×2 time-dependent positive definite symmetric matrix and $\boldsymbol{r}=(x,y)$. The angle $\theta_0(t)$ is the value of the θ angle along the beam axis. The matrix $Q(t)$ has three independent components uniquely related to the major axis length $\theta_1(t)$, the minor axis length $\theta_2(t)$, and the angle $\gamma(t)$ between the x axis and the major axis of the θ profile; $Q(t)$ is explicitly defined as

$$Q(t)=\begin{pmatrix} \dfrac{\cos^2\gamma(t)}{\theta_1^2(t)}+\dfrac{\sin^2\gamma(t)}{\theta_2^2(t)} & \left(\dfrac{1}{\theta_1^2(t)}-\dfrac{1}{\theta_2^2(t)}\right)\sin\gamma(t)\cos\gamma(t) \\ \left(\dfrac{1}{\theta_1^2(t)}-\dfrac{1}{\theta_2^2(t)}\right)\sin\gamma(t)\cos\gamma(t) & \dfrac{\sin^2\gamma(t)}{\theta_1^2(t)}+\dfrac{\cos^2\gamma(t)}{\theta_2^2(t)} \end{pmatrix}. \tag{5}$$

The axes lengths $\theta_1(t)$ and $\theta_2(t)$ are defined at $1/e$ of the maximum value θ_0 of the θ profile. In this way, the whole reorientation in the sample is parametrized by six time-dependent quantities (p_α, $\alpha=1,\ldots,6$), each endowed with a simple physical meaning: $\theta_0(t),\phi_0(t),\phi_1(t),\gamma(t),\ \theta_1(t),\ \theta_2(t)$. Out of equilibrium, the dynamical equations governing the evolution of these quantities were deduced by means of Ritz's variational method for dissipative systems [26], i.e.,

$$\frac{\partial\mathcal{F}}{\partial p_\alpha}=\frac{\partial\mathcal{R}}{\partial\dot{p}_\alpha}, \tag{6}$$

where the dot means the time derivative, and

$$\mathcal{F}=\frac{1}{2}\int_V dV[k_{11}(\mathrm{div}\boldsymbol{n})^2+k_{22}(\boldsymbol{n}\cdot\mathrm{rot}\boldsymbol{n})^2 + k_{33}(\boldsymbol{n}\times\mathrm{rot}\boldsymbol{n})^2-2w] \tag{7}$$

is the free energy of the system as a function of the parameters. $k_{ii}, i=1,2,$ and 3 are the LC elastic constants for splay, twist, and bend, respectively, and w is the density of electromagnetic energy in the sample volume V. In Eq. (6), $\mathcal{R}$ is the dissipative function, that, neglecting backflow, reduces to

$$\mathcal{R}=\frac{\gamma_1}{2}\int_V dV(\partial_t\boldsymbol{n}\cdot\partial_t\boldsymbol{n}), \tag{8}$$

where γ_1 is a viscosity coefficient. The electromagnetic energy density w in Eq. (7) is expressed as a function of $\boldsymbol{n}$, $I(x,y)$, and of the reduced Stokes vector $\boldsymbol{s}$ yielding the polarization of the optical field propagating in the LC film. In the geometric optics approximation (GOA) and in the small birefringence limit, w reduces to [18]

$$w=\frac{I(x,y)}{2c}[n_o+\{\overline{n}(\theta)-n_0\}(1+\boldsymbol{\Omega}\cdot\boldsymbol{s})], \tag{9}$$

where $\boldsymbol{\Omega}=(\cos2\phi,\sin2\phi,0)$, c is the speed of light in vacuum (cgs units are used), n_o is the LC ordinary refractive index, and $\overline{n}(\theta)$ is the refractive index seen by the extraordinary wave, given by

$$\overline{n}(\theta)=\frac{n_o n_e}{\sqrt{n_e^2\cos^2\theta+n_o^2\sin^2\theta}}=n_o+\frac{n_o(n_e^2-n_o^2)}{2n_e^2}\theta^2+o(\theta)^4, \tag{10}$$

where n_e is the extraordinary refractive index of the material. When the light traverses the LC film, its intensity profile $I(x,y)$ remains unchanged but its polarization may be strongly affected. In the case of normal incidence and very small twist deformation [$\phi_1(t)\ll1$], the GOA is prevailing and the equation governing the polarization state of the light can be cast in the precession form [18]

$$\frac{\partial\boldsymbol{s}}{\partial\alpha}=\boldsymbol{\Omega}\times\boldsymbol{s}, \tag{11}$$

where

$$\alpha=\frac{2\pi}{\lambda}\int_0^z dz[\overline{n}(\theta)-n_o] =\frac{n_o(n_e^2-n_0^2)}{4n_e^2\lambda}\left[2\pi z-L\sin\left(\frac{2\pi z}{L}\right)\right]\theta^2(x,y,t) \tag{12}$$

is the phase difference between the extraordinary and the ordinary wave in the given z plane, and λ is the light wavelength in vacuum. In evaluating the electromagnetic energy

$\mathcal{W}=\int_V w\,dV$, $\boldsymbol{s}$ is integrated over the transverse x,y plane with $I(x,y)$ as weight function. Only the central part of the beam contributes effectively to the integral, so we can solve Eq. (11) setting $x=y=0$. Then, the integration of Eq. (11) can be done analytically when $\theta_0(t)$ and $\phi_1(t)$ are small [25]. The ordinary differential equations (ODE) of our model have been obtained by inserting the solution of Eq. (11) and the ansatz (2), (3), and (4) into Eqs. (6) after having expanded the total free energy $\mathcal{F}$ up to the fourth order in the small parameters $\theta_0(t)$ and $\phi_1(t)$. The phase difference α, however, although proportional to θ_0^2, was not considered small, because it can range over several π even if $\theta_0 \ll 1$. The six ODE for the parameters p_α ($\alpha=1,\ldots,6$) are first order in time and they have been integrated numerically for different values of the control parameters P and β. The ODE are too long to be reported here in full and they will be discussed in deeper details in a forthcoming paper. A closer inspection in these equations shows, however, that the equations for the director azimuthal angle $\phi_0(t)$ and for the angle $\gamma(t)$ of the θ distribution describe the transfer of the spin and the orbital angular momentum from the light beam to the LC sample, respectively. The form of these two equations is

$$A(p_\alpha)\dot{\phi}_0 = -\frac{P}{\omega}\Delta s_3 + \tau_{int}, \tag{13}$$

$$B(p_\alpha)\dot{\gamma}(t) = -\frac{P_e}{\omega}\Delta L_z - \tau_{int}, \tag{14}$$

where A and B are functions of the other parameters, ω is the optical frequency, s_3 is the Stokes parameter measuring the average spin angular momentum per photon (in units of $\hbar$), and ΔL_z is the average orbital angular momentum transferred per photon (in units of $\hbar$), given by [27]

$$\Delta L_z = P^{-1}\int\int dxdy I(x,y)(x\partial_y - y\partial_x)\Delta\alpha(x,y). \tag{15}$$

In this equation, $\Delta\alpha(x,y)=\alpha(x,y,L)-\alpha(x,y,0)$ is the phase difference suffered by the extraordinary wave in traversing the sample given by Eq. (12) at $z=L$, and, in Eq. (14), P_e is the power carried out by the extraordinary wave only

$$P_e = P[1+\cos(2\phi_0(t)-\beta)]. \tag{16}$$

The ordinary wave does not contribute to the orbital angular momentum transfer because its phase change is uniform over the transverse plane. Both the ordinary and the extraordinary waves contribute instead to the polarization ellipticity change Δs_3. Small first-order terms in $\phi_1(t)$ have been neglected in Eq. (16), but they have been retained in the model. The presence of the torsion degree of freedom $\phi_1(t)$ in our model is essential, because, when omitted, the oscillating regimes, observed in the experiments, cannot be retrieved. Finally, we notice the presence of the torque τ_{int} in Eqs. (13) and (14). This torque is elastic in origin being proportional to the elastic anisotropy $\Delta k_{12}=k_{11}-k_{22}$ of the LC, and depends on the transverse gradients of $\boldsymbol{n}$. Its presence is due to the lack of invariance of $\mathcal{F}$ under separate infinitesimal rotations of the molecular director $\boldsymbol{n}(\boldsymbol{r})$ and of the center-of-mass $\boldsymbol{r}$ of the considered fluid element. In the plane-wave approximation, where $\boldsymbol{n}$ depends on the z coordinate only, τ_{int} vanishes and Eq. (13) reduces to the well known equation governing the transfer of the spin angular momentum to LC films [16]. When Eqs. (13) and (14) are added together, τ_{int} cancels out, being an internal torque, and we find that the rotational motion of the LC around the z axis is entirely governed by the total (spin+angular) momentum subtracted to the incident beam. In particular, at steady state when $\dot{\phi}=\dot{\gamma}=0$, the spin and the orbital part of the light angular momentum must balance each other. Both quantities depend on the phase change $\Delta\alpha$, so that the balance condition can be regarded as a transcendent equation for $\Delta\alpha$. Because Δs_3 has a period 2π as a function of $\Delta\alpha$, this equation has multiple solutions, yielding to the appearance of multiple steady states. Both model and experiment show that the different branches of steady states correspond to values of α roughly spaced by 2π. We may conclude therefore that the multistability of the system observed in the experiments originates from the balance between the spin and the orbital angular momentum of the light transferred to the sample at steady state.

III. THE EXPERIMENTAL RESULTS

In our experiments, we used a frequency doubled cw Nd:YVO_4 laser source, working at $\lambda=532$ nm. The sample was a 50-μm-thick E7 nematic film sandwiched between glass covers coated with DMOAP for strong homeotropic alignment. The laser intensity profile at the sample position was made elliptical by using two cylindrical lenses with focal lengths $f_x=500$ mm and $f_y=30$ mm in the x and y directions, respectively. The beam radii ($1/e^2$ intensity) at the lens common focal plane were found to be $w_x=(178\pm5)$ μm and $w_y=(12\pm3)$ μm, corresponding to a profile ellipticity $\mu=w_x/w_y\approx15$. Our detection apparatus has already been described in detail elsewhere [28], and we sketch here its main features only. A charge-coupled device camera and a rotating polarizer were used, respectively, to provide simultaneous and real time measurements of the angular aperture Θ and of the polarization direction angle Φ of the far-field self-diffraction ring pattern, which formed beyond the LC sample when reorientation took place. For small LC distortion we have $\approx\Theta\propto\alpha$ and $\Phi\simeq\phi_0$, where α is the phase change in the sample and ϕ_0 is the azimuthal angle of the molecular director $\boldsymbol{n}$, averaged over the sample thickness [28]. The angles Θ and Φ provide roughly independent degrees of freedom of $\boldsymbol{n}$. Our measurements were performed using linearly polarized light and changing the power P incident on the sample and the polarization angle β. The variation of β was achieved manually rotating a $\lambda/2$ plate on purpose inserted in the experimental apparatus. From these data and from the geometry of the experimental setup α and ϕ were deduced. In Fig. 2 the observed dynamical regimes have been reported in the plane of the control parameters P and β. The threshold power P_{th} needed to induce the optical reorientation from the undistorted state as a function of the angle β is also shown (continuous line)

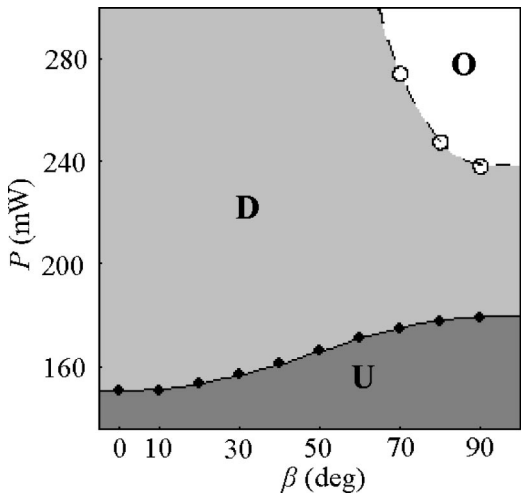

FIG. 2. Map of the dynamical regimes in the parameter plane P, β. Three regions may be recognized: **U**, undistorted states; **D**, steady distorted states; **O**, oscillating states. The continuous curve represents the thresholds for the OFT and the dashed curve represents the thresholds for the oscillations start up as calculated from our model. Full circles on the first curve and open circle on the second are the experimental points.

together with a second critical power curve (dashed line) delimiting a zone corresponding to nonlinear oscillations of ***n***. The dots are from experiments and the lines are from theory. All theoretical points were calculated using tabulated values for the material constants ($n_e=1.732$, $n_o=1.524$, $k_1=11.09\cdot10^{-7}$ dyn, $k_2=5.82\times10^{-7}$ dyn, $k_3=15.97\times10^{-7}$ dyn, $\gamma_1=1.9$ dyn sec/cm^2). The threshold power increases with β and reaches its maximum when the light polarization is perpendicular to the major axis of the intensity profile. The increasing of the threshold power with β is expected because of the competition between the spin and the orbital angular momentum of light: when $\beta=0$ they cooperate in reorienting the LC and the threshold power is minimum. From the threshold data, we extrapolated the threshold intensity in the plane-wave limit, obtaining $I_{th}=5.2$ kW/cm^2, which is in good agreement with the theoretical value $I_{th}=ck_3n_e^2\pi^2/[n_o(n_e^2-n_o^2)L^2]=5.5$ kW/cm^2. Starting from the undistorted state, the dynamical variables were found to reach their asymptotic values in a distorted state monotonically in time with a time constant $\tau=27$ s, in

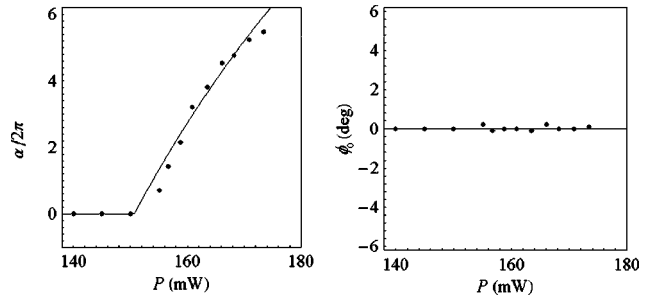

FIG. 3. The steady state values of α and ϕ_0 as functions of the incident power P for $\beta=0°$. Full circles are from experiment and full lines from theory.

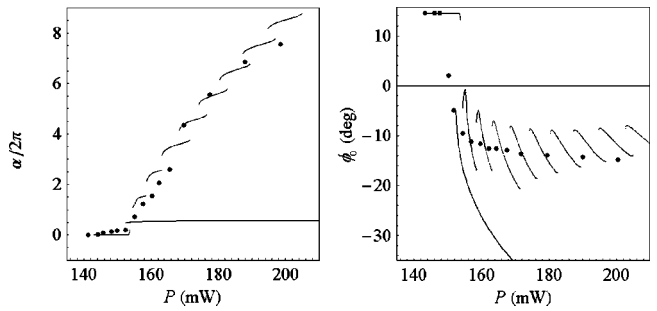

FIG. 4. The steady state values of α and ϕ_0 as functions of the incident power P for $\beta=20°$. Full circles are from experiment and full lines from theory.

good agreement with the theoretical value $\tau=\gamma_1L^2/k_{33}=30$ s. The transition from the undistorted state to the reoriented state at $P\gtrsim P_{th}$ is foreseen to be second order by the model, but this cannot be tested in our experiments, especially for high values of β, because of the low resolution in changing the incident laser power (≈2 mW) and because of the tendency exhibited by the system to jump through a first-order transition into other stable branches. We made our measurements from $\beta=0$ to $\beta=90°$ in steps of 10°. Figures 3–7 show the regime values of α and ϕ_0 as functions of the incident power P for $\beta=0°$, 20°, 50°, 70°, 90°. The theoretical curves were obtained upon directly integrating Eq. (6) in time up to $t=100\tau$, conveniently changing the initial conditions and the control parameters. This procedure allowed us to reconstruct the map of the stable steady states as well as of the oscillating states. The oscillating regimes appear in the figures as clouds of points within a zone measuring the oscillation amplitude. The occurrence of multiple steady states is clear from the theory (full lines) and confirmed by our experiments (dots), as shown in Figs. 3–7. Retracing experimentally the *plateau* foreseen by our model, however, is very difficult. When the power of the incident beam was changed, in fact, the system usually evolves into neighboring branches of steady states. Due to the fluctuation of the laser power ($\sim3\%$ nominal), we were not able to increase the power by steps less than 2 mW large. For this reason, the experimental points appear randomly located on different branches, as it is clearly shown in Fig. 5. It is remarkable, however, that the experimental points for α and ϕ_0 locate on corresponding branches.

In the case $\beta=0$ shown if Fig. 3, there is one branch and

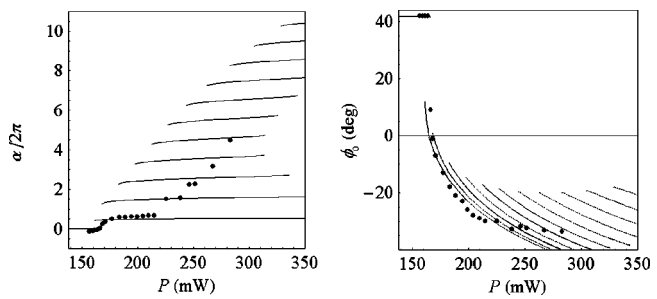

FIG. 5. The steady state values of α and ϕ_0 as functions of the incident power P for $\beta=50°$. Full circles are from experiment and full lines from theory.

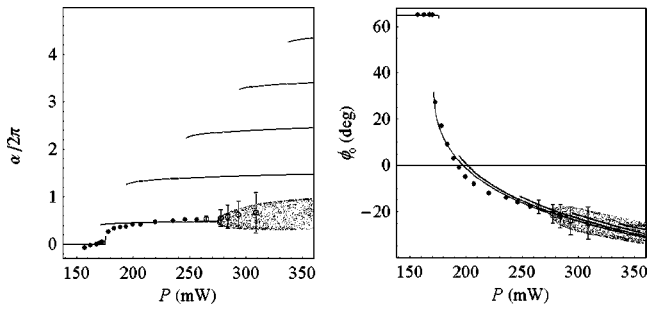

FIG. 6. The steady state values of α and ϕ_0 as functions of the incident power P for $\beta=70°$. Full and open circles are from experiment: the first ones represent steady states, the second ones oscillating states. The error bars measure the oscillation amplitude. Full lines are from theory.

the experimental points fit quite well with the calculated curves. In this case, the reorientation process is very similar to the usual OFT: above the threshold P_{th}, α ($\propto\theta_0^2$) increases monotonically as a function of P and ϕ_0 remains close to zero, confirming that the reorientation occurs in the plane of the beam polarization (along the optical E field). For $\beta\neq0$ several branches of stable steady states appear both for α and ϕ_0, which moves out of the light polarization plane. Except the lowest branch ($\alpha\approx\pi$), all other branches correspond to 2π jumps of α (see Figs. 5 and 6). Oscillatory regimes were observed when $\beta\gtrsim60°$ within the explored range of P (see Figs. 6–8).

In the presence of multistability, the fitting to the experimental data was difficult, because the experimental points were randomly distributed on different branches. Nevertheless, we were facilitated by the constraint to locate the experimental data for α and ϕ_0 on corresponding branches. Numerical simulations showed that the dynamical regimes exhibit both qualitative and quantitative aspects which depend dramatically on the size of w_x and w_y. On both a theoretical and an experimental level, it would be desirable having at our disposal a detailed analysis with respect to these parameters, which is to be dealt with in a future work.

At $\beta=90°$, in particular, two main effects appear which make the situation particularly intriguing. First, as the power P is increased, oscillations tend to become irregular. Second,

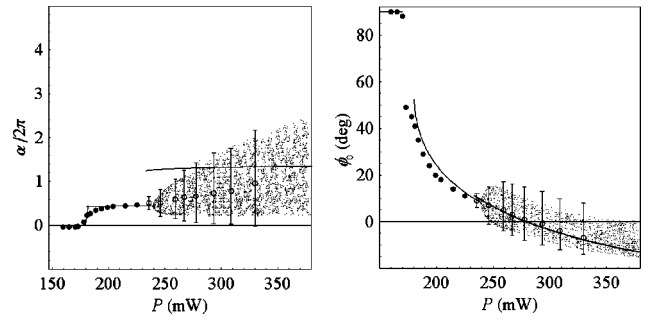

FIG. 7. The steady state values of α and ϕ_0 as functions of the incident power P for $\beta=90°$. Full and open circles are from experiment: the first ones represent steady states, the second ones oscillating states. The error bars measure the oscillation amplitude. Full lines are from theory.

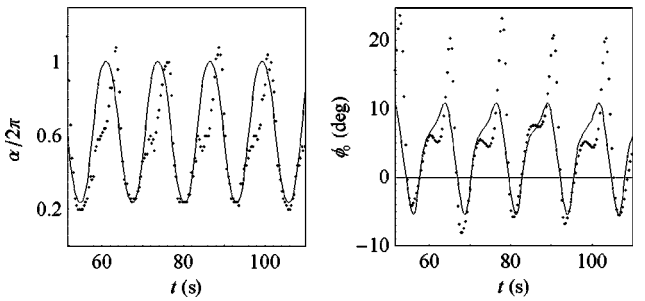

FIG. 8. Example of persistent time oscillation at $\beta=90°$ and $P=260$ mW. The dots are from experiment and the full line is from theory.

as the power P is decreased, starting from an oscillatory state, the system tends to evolve into a stationary state, such as the one embedded in the cloud of points in Fig. 7.

Finally, an instance of oscillatory regime for α and ϕ_0 is shown in Fig. 8, where the experimental data are superimposed on the theoretical curves.

IV. CONCLUSIONS

We presented a study on the OFT induced in homeotropically aligned nematic LC by a linearly polarized laser beam having elliptical rather than circular transverse profile. The data were taken as functions of the incident laser power P and of the angle β between the beam polarization direction and the major axis of the beam profile. Above the threshold to induce the molecular reorientation, we observed the occurrence of multiple steady states and of oscillating dynamical regimes at large values of β. The oscillating regimes can be excited only when the incident power exceeds a second critical threshold and $\beta\gtrsim60°$. At $\beta=90°$ the oscillations become irregular when the incident power is further increased. A more detailed study of these irregular dynamical regimes will be postponed to an incoming work. At $\beta=0$ the reorientation process is very similar to the standard OFT and the reorientation takes place in the polarization plane of the incident beam. When $\beta\neq0$, the reorientation is out of the light polarization plane and, above the OFT threshold, multiple steady states were always observed. Multistability and oscillating regimes were never reported in the standard OFT. We worked out also a model based on Ritz's variational method applied to the total (elastic+optical) free energy. The model assumes elongated Gaussian profiles for the incident beam profile and for the profile of the zenithal angle θ of the molecular director. All space coordinates and time were retained (within a simplified model) and the elastic anisotropy of the material was taken also into account. In spite of the approximations involved, our model was able to predict the occurrence of multiple steady states and of the observed oscillations of the molecular director. The overall physical picture emerging from our model is that the main features of the observed phenomena are due to the delicate interplay between the orbital and the spin parts of the angular momentum extracted from the incident light beam. In particular, owing to the homeotropic anchoring at the walls, steady states can be reached only when the orbital and the spin

angular momentum transferred to the sample balance to zero. This forces the phase change α of the optical wave to assume values spaced of 2π, yielding multistability. The transitions between multistable states was predicted (and observed) to be first order, although the early Fréedericksz transition from the undistorted state to the first distorted state was predicted to be second order. Numerical simulations showed a strong dependence of the dynamical regimes on the transverse dimensions of the incident laser beam. Further study in this direction would be devisable. Due to unavoidable fluctuations of the laser power, we were unable to explore in great details the different branches of stable states, because of the tendency of the system to jump randomly from one branch to the other. A better control of the multistability would be also devisable, because of potential applications. Finally, all points of the theoretical curves shown in the figures have been determined by directly integrating our ODE in time. This procedure, although straightforward, is very time consuming and we cannot be sure that some solutions were missing. A detailed and systematic analysis of our ODE using more powerful analytical and numerical tools will be the object of future investigation.

ACKNOWLEDGMENTS

We thank INFM (Istituto Nazionale per la Fisica della Materia) and MIUR (Ministero dell'Istruzione, Università e Ricerca) for financial support.

[1] A.S. Zolot'ko, V.F. Kitaeva, N. Kroo, N.I. Sobolev, and L. Csillag, Pis'ma Zh. Éksp. Teor. Fiz. **32**, 170 (1980) [JETP Lett. **32**, 158 (1980)].
[2] S.D. Durbin, S.M. Arakelian, and Y.R. Shen, Phys. Rev. Lett. **47**, 1411 (1981).
[3] I.C. Khoo and S.T. Wu, *Optics and Nonlinear Optics of Liquid Crystals* (World Scientific, Singapore, 1993), Vol. 1.
[4] L. Marrucci and Y.R. Shen, in *The Optics of Thermotropic Liquid Crystals*, edited by R. Sambles and S. Elston (Taylor and Francis, London, 1997).
[5] E. Santamato and Y.R. Shen, in *A Guide to Liquid Crystal Research*, edited by P.J. Collings and J.S. Patel (Oxford University Press, New York, 1997), Chap. 14, pp. 539–566.
[6] V. Fréedericksz and V. Zolina, Trans. Faraday Soc. **29**, 919 (1933).
[7] A.J. Karn, S.M. Arakelian, Y.R. Shen, and H.L. Ong, Phys. Rev. Lett. **57**, 448 (1986).
[8] E. Santamato, G. Abbate, R. Calaselice, P. Maddalena, and A. Sasso, Phys. Rev. A **37**, 1375 (1988).
[9] G. Abbate, A. Ferraiuolo, P. Maddalena, L. Marrucci, and E. Santamato, Liq. Cryst. **14**, 1431 (1993).
[10] M.-M. Cheung, S.D. Durbin, and Y.R. Shen, Opt. Lett. **8**, 39 (1983).
[11] P.-Y. Wang, H.-J. Zhang, and J.-H. Dai, Opt. Lett. **12**, 654 (1987).
[12] M.G. Clerc, S. Residori, and C.S. Riera, Phys. Rev. E **63**, 060701 (2001).
[13] L. Marrucci, F. Vetrano, and E. Santamato, Opt. Commun. **171**, 131 (1999).
[14] L. Marrucci, B. Piccirillo, and E. Santamato, J. Opt. A, Pure Appl. Opt. **2**, 294 (2000).
[15] B. Piccirillo, C. Toscano, F. Vetrano, and E. Santamato, Phys. Rev. Lett. **86**, 2285 (2001).
[16] E. Santamato, B. Daino, M. Romagnoli, M. Settembre, and Y.R. Shen, Phys. Rev. Lett. **57**, 2423 (1986).
[17] E. Santamato, M. Romagnoli, M. Settembre, B. Daino, and Y.R. Shen, Phys. Rev. Lett. **61**, 113 (1988).
[18] E. Santamato, G. Abbate, and P. Maddalena, Phys. Rev. A **38**, 4323 (1988).
[19] T.V. Galstyan and V. Drnoyan, Phys. Rev. Lett. **78**, 2760 (1997).
[20] G. Abbate, P. Maddalena, L. Marrucci, L. Saetta, and E. Santamato, Phys. Scr., T **39**, 389 (1991).
[21] A.S. Zolot'ko, V.F. Kitaeva, N.N. Sobolev, and A.P. Sukhorukov, Zh. Éksp. Teor. Fiz. **81**, 933 (1981) [Sov. Phys. JETP **54**, 496 (1981)].
[22] I.C. Khoo, T.H. Liu, and P.Y. Yan, J. Opt. Soc. Am. B **4**, 115 (1987).
[23] B.Y. Zel'dovich and N.V. Tabiryan, Zh. Éksp. Teor. Fiz. **82**, 1126 (1982) [Sov. Phys. JETP **55**, 656 (1982)].
[24] M.A. Karpierz, M. Sierakowski, and T.R. Wolinkski, Mol. Cryst. Liq. Cryst. **375**, 313 (2002).
[25] A. Vella, B. Piccirillo, and E. Santamato, Phys. Rev. E **65**, 031706 (2002).
[26] S. Subota, V. Reshetnyak, and M.S. Soskin, Mol. Cryst. Liq. Cryst. Sci. Technol., Sect. A **375**, 481 (2002).
[27] S.J. van Enk and G. Nienhuis, Opt. Commun. **94**, 147 (1992).
[28] E. Santamato, G. Abbate, P. Maddalena, L. Marrucci, D. Paparo, and B. Piccirillo, Mol. Cryst. Liq. Cryst. **328**, 479 (1999).